# Optimal Reactor Network for Methanol Synthesis Using RCC Algorithm for Attainable Regions Analysis

Tumisang Seodigeng, and Guida Muala

***Abstract* —** Optimal reactor network for methanol synthesis over Cu-Zn-Al catalyst has been developed by automated attainable regions analysis using the recursive convex control policy algorithm. Fundamental processes of solid catalysed gaseous reaction, cooling, mixing and heating are considered in order to develop a reactor network that can be used to attain specific optimal conditions such as maximum conversion or minimisation of the required heating or cooling surface area.

***Keywords*—** Attainable regions, Methanol synthesis, Optimal reactor networks, Recursive Convex Control policy algorithm.

## I. Introduction

TTAINABLE REGIONS ANALYSIS is a process synthesis and optimization method that can be used develop optimal reactor networks by considering application onto the given feed, of all permitted processes that can be used to transform the feed to the required product such as reaction, mixing , heating and separation [1]–[3]. The Attainable Region (AR) is defined as a set of all possible outcome states that can be realised from all or any feasible combination of all permitted fundamental processes for a given input, subject to specified constraints. The boundary of the AR sets limits to the achievable states and it is therefore of special interest as it is where the optimal operating policies can be located [4]–[6]. Numerous researchers have spent the past two decades developing a theory to define and characterise the completeness of the AR. Feinberg developed a number of rigorous geometric theorems that can be used as necessary conditions for a given region to be deemed as the attainable region [7]–[8]. Manousiouthakis *et al.* [9] derived a necessary and sufficient condition for the attainable region.

Recent research on attainable regions analysis has focused on developing systematic computational algorithms or tools that can be used to automate the development and interpretation of attainable regions [10]–[16]. Most of the techniques developed focused mainly on the generation of the attainable region from the fundamental principles. Once the region is obtained, optimisation on the boundary of the region can be performed by satisfying the objective function. However, these techniques offered no help on the interpretation of the optimal point on the boundary of the AR as a network of interconnected processes that can further be interpreted as unit operations of reactions, mas transfer and heat transfer with specified key design parameter.

Seodigeng et al. [17] developed the recursive convex control (RCC) policy algorithm for attainable regions that could be used to systematically develop the AR for a given feed system and permitted fundamental processes and further interpret all the points on the attainable regions as a series of fundamental processes that can be used to attain any product point on the AR from the feed. This network of fundamental process could then be easily translated into a process flowsheet comprising interconnected unit operations with design parameters such as reactor residence times and heat transfer areas.

## II. Methanol Synthesis Background

In this work we will identify optimal reactor networks for low-pressure methanol synthesis. Low pressure methanol synthesis has been for many years understood to form from the reaction of carbon monoxide and hydrogen by most researchers [18]–[21]. The reaction for methanol synthesis from CO is given by,

$$CO + 2H_2 \leftrightarrow CH_3OH \qquad \Delta H^{\circ}_{298} = -90.64 \text{ kJ mol}^{-1} \qquad (I)$$

For this proposed reaction route the role of $CO_2$ in methanol synthesis was considered to be and restricted to competitive adsorption on the active sites of the catalysts. Some researchers contrary to this claimed that methanol is formed from $CO_2$ only due to its strong adsorption power, subduing and inhibiting the co-adsorption of CO [22]–[23]. It was only in the past two decades that researchers started to assimilate the role of $CO_2$ together with that of CO in methanol synthesis reaction models. Denise and Sneeden [24] and Klier *et al.* [26] proposed a kinetic model incorporating both CO and $CO_2$ reactions from conclusions based on kinetic experiments. Liu *et al*. [27] came to the same conclusion based on experiments

Tumisang Seodigeng is with the Department of Chemical Engineering, University of Johannesburg, Doornfontein Campus, Johannesburg 2028, South Africa (corresponding author phone: +27 11 559 6527; fax: +27 86 225 7232; e-mail: tseodigeng@uj.ac.za ).

Guida Muala is with the Department of Chemical Engineering, University of Johannesburg, Doornfontein Campus, Johannesburg 2028, South Afica (e-mail: mualaguida@yahoo.com).

with labelled oxygen in $CO_2$. Graaf *et al.* [25] proposed a fully incorporating kinetic model which considered the two reactions over a Cu-Zn-Al catalyst. In their model they also considered this catalyst for being known to promote the water-gas-shift (WGS) reaction as the third reaction. Struis and Stucki [29],[30] reviewed the kinetic models proposed by Graaf *et al.* [25] with modification for their study of membrane reactor concept for methanol synthesis.

In this work we apply attainable regions analysis to the modified Graaf *et al.* [25] kinetic models to identify optimal reactor network for methanol synthesis. We start by first studying the kinetics in detail to investigate if there are any evident optimal structures to be expected and then apply automated techniques to identify optimal reactor structures which can further be compared to prior expectations.

## III. Methanol Synthesis: The Kinetics

The kinetic model used in this study is that of Graaf *et al.* [25] as modified by Struis and Stucki [30]. Methanol synthesis comprises three equilibrium limited reactions as shown below

$CO + 2H_2 \leftrightarrow CH_3OH$ $\quad \Delta H^{\circ}_{298} = -90.64$ kJ mol$^{-1}$ (I)
$CO_2 + H_2 \leftrightarrow CO + H_2O$ $\quad \Delta H^{\circ}_{298} = 41.17$ kJ mol$^{-1}$ (II)
$CO_2 + 3H_2 \leftrightarrow CH_3OH + H_2O$ $\quad \Delta H^{\circ}_{298} = -49.47$ kJ mol$^{-1}$ (III)

The two reactions for methanol formation (I) and (III), are exothermic as written, and are influenced towards the product side by high pressures. The WGS reaction, (II) is endothermic and its equilibrium is not a function of pressure as the number of moles does not change as the reaction occurs. For reactions (I) and (III), high temperatures are required for high rates of reaction whilst high equilibrium conversion is favoured by low temperatures, a general trend observed with exothermic reversible reactions. However, the WGS reaction is endothermic as written and therefore favours high temperatures for both reaction rates and high equilibrium conversion.

Graaf *et al.* [25] derived the kinetic rate expressions for each of the three reactions, by defining chemical reaction as the rate controlling step and advocated the adsorption mechanism to be a dual-site Langmuir-Hinshelwood mechanism, where CO, $CO_2$, $H_2$ and $H_2O$ can all adsorb competitively. The rates of formation of species in the reaction system are given by Graaf *et al.* [25] as;

$$r'_{CH_3OH,1} = \frac{k'_{ps,1}K_{CO}\left[f_{CO}f_{H_2}^{3/2} - f_{CH_3OH}/\left(f_{H_2}^{1/2}K^{o}_{p1}\right)\right]}{\left(1+K_{CO}f_{CO}+K_{CO_2}f_{CO_2}\right)\left[f_{H_2}^{1/2}+\left(K_{H_2O}/k_{H_2}^{1/2}\right)f_{H_2O}\right]} \quad (1)$$

$$r'_{H_2O,2} = \frac{k'_{ps,2}K_{CO_2}\left(f_{CO_2}f_{H_2} - f_{H_2O}f_{CO}/K^{o}_{p2}\right)}{\left(1+K_{CO}f_{CO}+K_{CO_2}f_{CO_2}\right)\left[f_{H_2}^{1/2}+\left(K_{H_2O}/k_{H_2}^{1/2}\right)f_{H_2O}\right]} \quad (2)$$

$$r'_{CH_3OH,3} = \frac{k'_{ps,3}K_{CO_2}\left[f_{CO_2}f_{H_2}^{3/2} - f_{CH_3OH}f_{H_2O}/(f_{H_2}^{3/2}K^{o}_{p3}\right]}{\left(1+K_{CO}f_{CO}+K_{CO_2}f_{CO_2}\right)\left[f_{H_2}^{1/2}+\left(K_{H_2O}/k_{H_2}^{1/2}\right)f_{H_2O}\right]} \quad (3)$$

The gas composition is given by fugacities ($f_i$) for each gas species *i* (in pressure units: bar). For the purpose of this study the fugacities shall be considered to be adequately approximated by partial pressures and this assumption will be carried henceforth. The adsorption equilibrium constants are symbolised by $K_{CO}$, $K_{CO2}$, $K_{H_2}$ and $K_{H_2O}$ respectively, and chemical equilibrium constants for the three reactions are denoted by $K^0_{p_1}$, $K^0_{p_2}$ and $K^0_{p_3}$, respectively, with subscripts *p* indicating that these constants are based on partial pressure. Each reaction rate, $r_j$, is characterised by a rate constant, $k'_{ps,j}$, where subscript *j* refers to the consigned reaction (viz. j = 1, 2, 3 for reaction (I), (II), (III) respectively). The chemical equilibrium constants are reported by Struis and Stucki (2001) as

$$K^{o}_{p_1} = 10^{(3921/T)-7.971\times^{10}\log(T)+2.499\times10^{-3}\times T-2.953\times10^{-7}\times T^2+10.20} \quad (4)$$

$$K^{o}_{p_2} = 10^{6.959-(2489/T)-1.565\times^{10}\log(T)+6.6\times10^{-5}\times T+(2.3\times10^{4}/T^2)} \quad (5)$$

$$K^{0}_{p_3} = K^{0}_{p_1}\cdot K^{0}_{p_2} \quad (6)$$

The modified parameters for the Graaf *et al.* [25] kinetic model were resolved by Struis and Stucki [30] as the following;

$$k'_{ps,1} = (1.23\pm0.17)\times10^{6}\exp(-104430\pm3110/RT) \quad (7)$$
$$k'_{ps,2} = (2.21\pm0.13)\times10^{10}\exp(-123500\pm1450/RT) \quad (8)$$
$$k'_{ps,3} = (3.390\pm0.080)\times10^{3}\exp(-65250\pm430/RT) \quad (9)$$
$$K_{CO} = (9.72\pm0.38)\times10^{-7}\exp(57260\pm590/RT) \quad (10)$$
$$K_{CO_2} = (1.190\pm0.050)\times10^{-7}\exp(66710\pm670/RT) \quad (11)$$
$$(K_{H_2O}/K^{1/2}_{H_2}) = (4.14\pm0.10)\times10^{-11}\exp(104500\pm525/RT) \quad (12)$$

The model parameters were fitted for the experimental conditions within the range of T =200-260˚C and P = 30-60 bar. However, the Cu-Zn-Al catalyst is known to be active for the three methanol synthesis reactions in the temperature range T = 400 – 600K [31].

For a feed mixture of CO and $CO_2$ in mole ratio of 1:1 and the stoichiometric amount of $H_2$, the following chemical equilibrium curves can be established at various outlet pressures as indicated in Figure 1. The molar composition of the feed for this case can be evaluated as [$CH_3OH$ CO $CO_2$ $H_2$ $H_2O$] = [0 0.14 0.14 0.72 0].

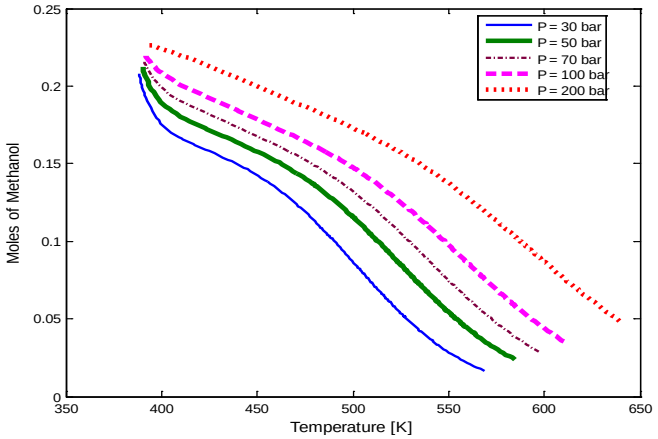


Fig. 1: Variation of chemical equilibrium with pressure

In agreement with the expectations, the equilibrium conversion of methanol increases with increasing pressure at a specified temperature. This behaviour is as stated earlier, due to the fact that the methanol forming reactions; (I) and (III), both result in decreased total number of moles and therefore high pressure will favour conversion towards the product. Figure 2 shows how the equilibrium composition of methanol changes as the mole ratio of $CO_2$: CO is varied. The observed trend is that the equilibrium amount of methanol decreases as the ratio of CO decreases. This observation could be attributed to the fact that CO has a higher tendency to react to form methanol than $CO_2$. To investigate this proposal the average rate contours are used to study the kinetics in more detail. The rate contour study is carried out at a fixed pressure of 50 bar using the feed gas composition as stated above.

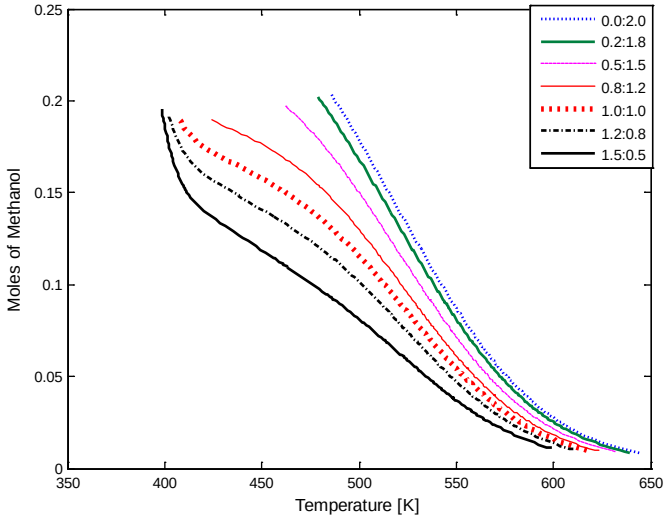


Fig. 2: Variation of chemical equilibrium with $CO_2$:CO mole ratio

The average rate contours for formation of methanol are shown in Figure 3. The rate contours plotted are the summed individual rates of formation of methanol from reaction (I) and (III) as defined by expressions (1) and (3) respectively. In this case, the WGS reaction (II) is not considered. The rates as quoted are in units of $mol \cdot s^{-1} \cdot kg\text{-}catalyst^{-1}$. Figure 4 depicts contours for the rate of formation of methanol from CO (reaction I). By comparison of magnitude with rate of formation of methanol from both CO and $CO_2$ (Figure 3), it appears that methanol is likely to form mainly from CO through reaction (I). This observation is supported by the low rate values of formation of methanol from $CO_2$ as shown in Figure 5, which are in the range of one-tenth of the combined effect in Figure 3.

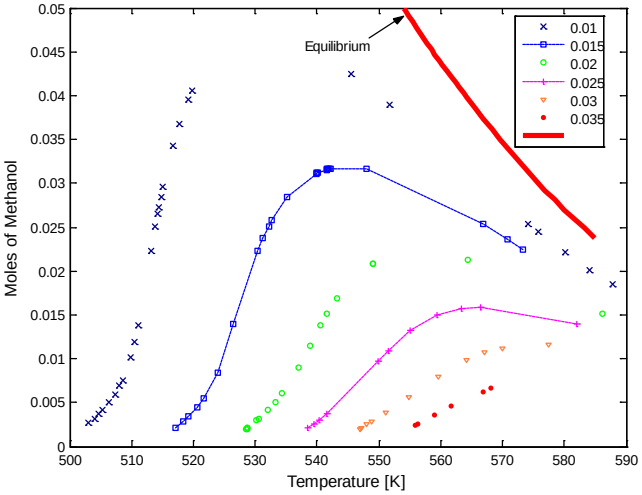


Figure 3: Average isorate contours for methanol formation ($r = r_{CH3OH,1} + r_{CH3OH,3}$)

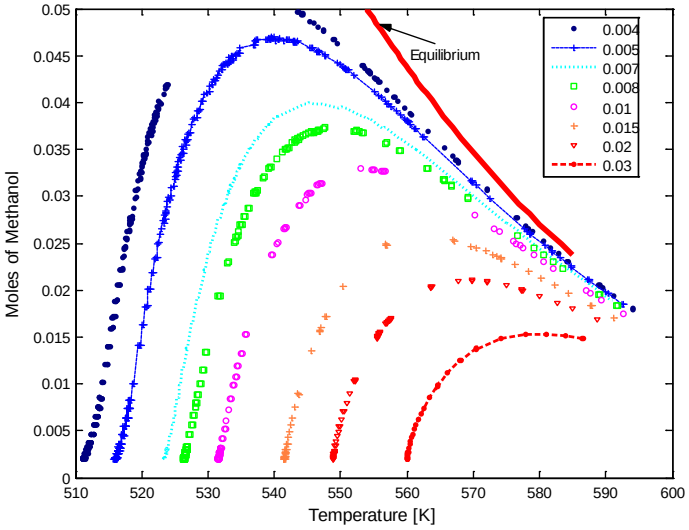


Fig. 4: Isorate contours for methanol formation from reaction (I) ($r = r_{CH3OH,1}$)

To investigate the effect of the WGS reaction, the contours for the rate of reaction of CO from reactions (I) and (II) are shown in Figure 6. The contours show an oval shape as compared to the S-shape of Figure 4. It can be seen from the slightly reduced rate of consumption of CO when compared to the trend in Figure 4 that the WGS reaction effects the formation CO. In the case where the WGS reaction is redundant, the contours in Figure 6 would resemble that in Figure 4.

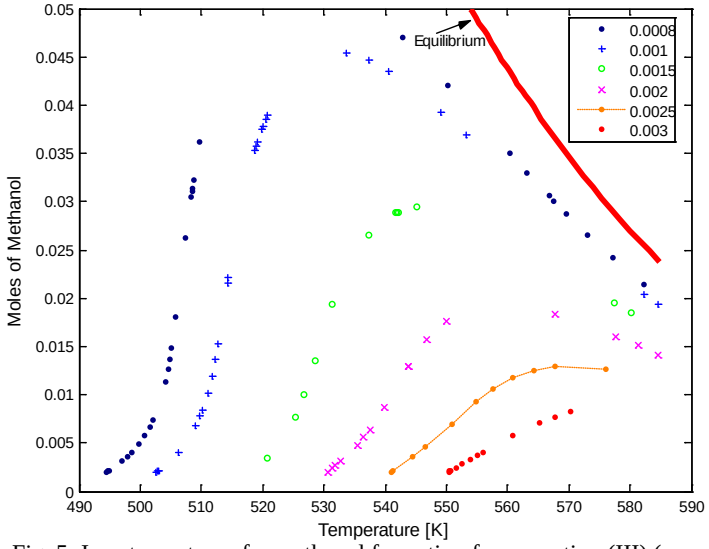


Fig. 5: Isorate contours for methanol formation from reaction (III) (r = $r_{CH3OH,3}$ )

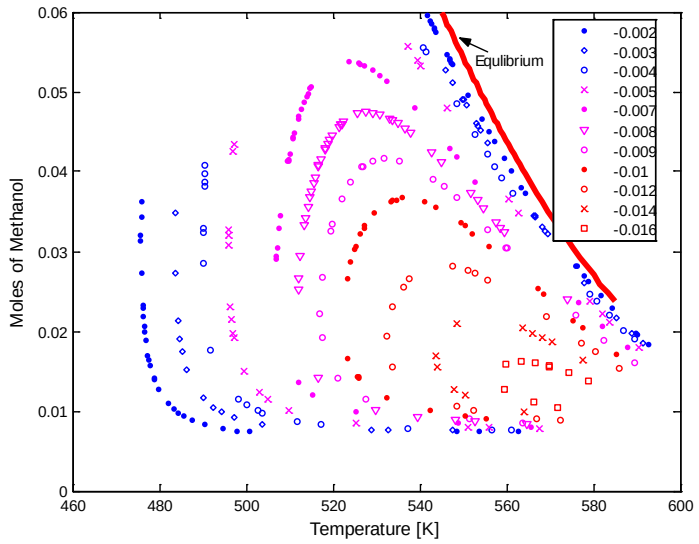


Fig. 6: Average isorate contours for CO reaction from reactions (I) and (II) (r = rCO,2 - rCO,1)

It is evident from the observation of the plots of rate contours that the determination of optimal reactor structures for methanol synthesis will not be clear-cut from a theoretical aspect as the optimum profiles of all three reactions have to be considered. In theory, the rate contours in Figure 3 for the average formation of methanol from reaction (I) and (III) could be used if the effect of the water gas shift reaction is considered insignificant. However, it can be noted in Figure 6 that the WGS reaction affects the reaction scheme in a considerable manner.

Depicted in Figure 7 are the adiabatic plug flow reactor profiles at varying feed temperature. These profiles show how the temperature changes with the mole fraction of methanol formed as the reaction system progresses. At low temperatures the reaction is exothermic as shown by the increase in temperature with increasing methanol conversion, giving an indication that the methanol forming reactions (I) and (III) are clearly dominating. As the reaction occurs the system gets more exothermic as indicated by the flattening of the PFR curves. At low methanol conversions and high temperatures (high feed temperature) the methanol reaction system becomes endothermic as indicated by the shaded area where the slope of the adiabatic PFR is negative indicating a decrease in temperature with increasing methanol conversion. In this region the endothermic WGS reaction (II) dominates. This behaviour is the expected trend with endothermic reactions as high temperatures favour both high rates of reaction and high equilibrium conversions.

This mixed exothermic-endothermic behaviour of the methanol synthesis system asserts that, the theoretical methods of determining optimum reaction-cooling and reaction-mixing profiles cannot be used to solve optimal reactor networks.

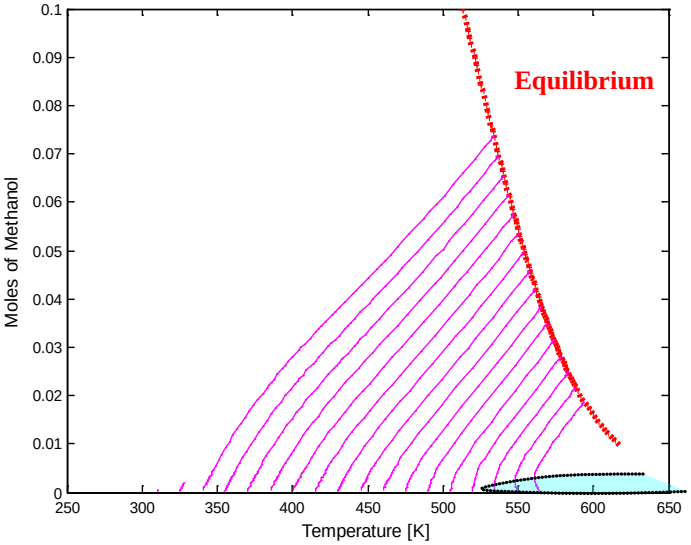


Fig. 7: Methanol synthesis adiabatic plug flow reactor profiles

In the next section we will formulate the RCC algorithm to solve the candidate AR for methanol synthesis using Graaf kinetics, from which the optimal profiles will be identified.

## IV. Methanol Synthesis: Problem Formulation

The permitted fundamental processes in this formulation of methanol synthesis are reaction, cooling, heating and mixing. The feed is provided at a temperature of 300K and is considered to be that of a 1:1 mixture of CO:$CO_2$ with the stoichiometric amount of hydrogen.

For the fundamental process of reaction all components that partake in the reaction are considered. A vector describing the rates of reaction of each component is given in (13). A vector associated with the rate of reaction of components is given by equation (13a)

$$r_m(m,T,\tau)=\begin{Bmatrix} r_1 = r_{CH_3OH} = r_I + r_{III} \\ r_2 = r_{CO} = -r_I + r_{II} \\ r_3 = r_{CO_2} = -r_{II} - r_{III} \\ r_4 = r_{H_2} = -2r_I - r_{II} - 3r_{III} \\ r_5 = r_{H_2O} = r_{II} \end{Bmatrix} \quad (13a)$$

The rates $r_I$, $r_{II}$ and $r_{III}$ are that of reactions (I), (II) and (III) as with expressions given by equations (1), (2) and (3) respectively. To describe the composition state, mass fraction of components; $m$ is used as a variable.

The vector describing the rate of change of temperature as the reaction occurs is given by equation (13b)

$$r_T(m,T,\tau) = \begin{Bmatrix} \mathrm{r}_1 \cdot T_{ad_1} \\ \mathrm{r}_2 \cdot T_{ad_2} \\ \mathrm{r}_3 \cdot T_{ad_3} \\ \mathrm{r}_4 \cdot T_{ad_4} \\ \mathrm{r}_5 \cdot T_{ad_5} \end{Bmatrix} \quad (13b)$$

And the rate associated with the change in residence time, $\tau$ is as described in the earlier chapters;

$$r_\tau(\tau) = \{1\} \quad (13c)$$

The general reaction vector for the system becomes

$$r(\boldsymbol{c}) = \begin{bmatrix} r_m(m,T,\tau) \\ r_T(m,T,\tau) \\ r_\tau(\tau) \end{bmatrix} \quad (14)$$

The characteristic vector of the system containing all variables that fully describe the system can now be defined as;

$$\boldsymbol{c} = \begin{bmatrix} m \\ T \\ \tau \end{bmatrix} \quad (15)$$

Mixing, cooling and heating vectors as previously shown are characterised by equations (16), (17) and (18) respectively.

$$v(\boldsymbol{c},\boldsymbol{c}_0) = \begin{bmatrix} m_0 - m \\ T_0 - T \\ \tau_0 - \tau \end{bmatrix} \quad (16)$$

$$k(\boldsymbol{c}) = \begin{bmatrix} 0 \\ K_c(T_c - T) \\ 0 \end{bmatrix} \quad (17)$$

$$h(\mathrm{c}) = \begin{bmatrix} 0 \\ K_h(T_h - T) \\ 0 \end{bmatrix} \quad (18)$$

Where mixing is performed with the mixing state $c_0 = [m_0, T_0, \tau_0]$ and cooling is assumed to be carried out using a constant temperature cooling utility at $T_c$. The heating utility temperature is symbolised as $T_h$. $K_c$ is to be a measure of the relative cost of cooling in comparison to cost of reaction. $K_h$ takes the analogous definition for heating.

The process combination vectors considered in this study are limited to combinations that always include reaction as one of the fundamental processes. Thus, the fundamental process of reaction will be included in all combinations. The vectors describing the combinations of processes are discussed in equation set (19) as follows.

Reaction and mixing are combined using the combination control policy $\alpha$, as represented in equation (19a) below;

$$g_{r,v} = r(c) + \alpha \cdot v(c,c_0) \quad (19a)$$

The process vector in equation (19b) shows the combination of fundamental processes of reaction and cooling using the control policy symbolised by $\beta$,

$$g_{r,k} = r(c) + \beta \cdot k(T,T_c) \quad (19b)$$

The combination control policy $\theta$, combines the processes of reaction and heating as represented by the combination vector given in equation (19c) below;

$$g_{r,h} = r(c) + \theta \cdot h(T,T_h) \quad (19c)$$

The general process vector for combination of all permitted fundamental processes in the system can then be expressed by as;

$$g_{r,v,k,h} = r(c) + \alpha_g \cdot v(c,c_0) + \beta_g \cdot k(T,T_c) + \theta_g \cdot h(T,T_h) \quad (20)$$

The subscript $g$ in the control policies indicates that the control policies are for the general process vector and not for the paired combinations as in (19). This will help differentiate between the general process vector and the paired combinations.

Given the problem specifications such as variable constraints, feed specifications, heating and cooling relative cost factors, utility limitations, *etc*, the RCC algorithm for the problem can now be formulated and implemented in MATLAB® to solve the optimal profiles of combinations of permitted fundamental processes and complete $AR^C$ for the methanol synthesis problem. The $AR^C$ boundary can further be interpreted as a sequence of application of fundamental processes and/or combinations thereof, which are applied to the feed states to attain the product states that shape the boundary. This interpretation is useful as the sequences of applied fundamental process and/or their combinations can be further interpreted into unit operations with design key parameters with essentially specifies the optimal process flowsheet.

## V. RESULTS

The primary objective of the two case studies detailed herein is to investigate the effect of cooling and heating relative cost factors on the shape of the $AR^C$ boundary and the

occurrence of combinations of fundamental processes on the boundary.

The feed to the system is, as stated earlier, to be a mixture of CO and $CO_2$ in mole ratio of 1:1 and the stoichiometric amount of $H_2$ resulting in molar composition of [$CH_3OH$ CO $CO_2$ $H_2$ $H_2O$] = [0 0.14 0.14 0.72 0]. The feed is available at the temperature of 300K. The system pressure is taken to be 50bar and assumed to remain constant as the reaction occurs for simplification purposes. The catalyst activity range is adopted from Twigg [31] to be between 400K and 600K. Cooling can be carried out to a minimum temperature of 300K as may be limited by the cooling utility temperature. Heating is similarly limited to a maximum of 600K.

*A. Case 1*

The cooling and heating relative cost factors $K_c$ and $K_h$, are taken to be equal at a fixed value of 500 with corresponding time units. This value is arbitrarily chosen. The reasoning behind the choice of this value is that the study does not aim at comparing the costs of heating and cooling to that of reaction, but instead investigate how the $AR^C$ boundary changes as the relative (to one another) costs of cooling and heating change.

Using the process specifications the $AR^C$ was solved in the 3D carbon conversion-residence time-temperature space and the results are show in Figure 8 on a Temperature-Conversion (T-X) 2D projection.

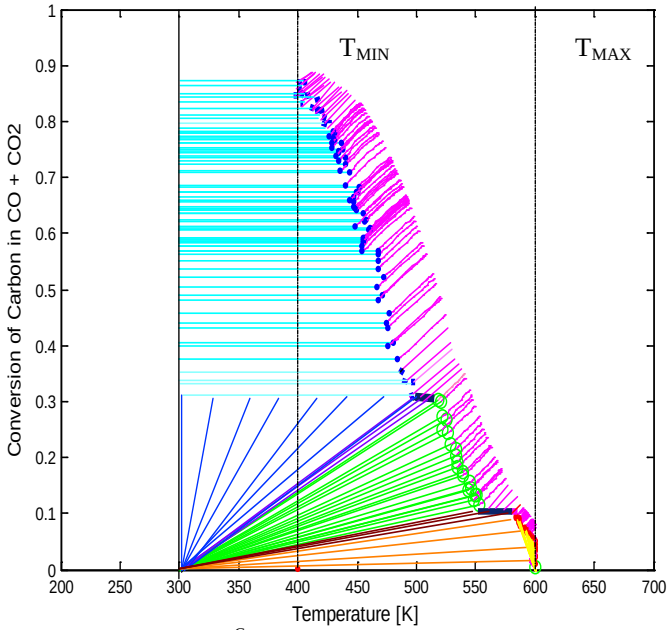


Fig. 8: A 2D T-X $AR^C$ Projection of Methanol Synthesis Case 1

Carbon conversion is defined as the mole fraction of carbon atoms (from both CO and $CO_2$) that reacted to form methanol.

The interpretation of the $AR^C$ boundary as a sequence of unit operations is enabled by a fully labelled boundary depicted in Figure 9.

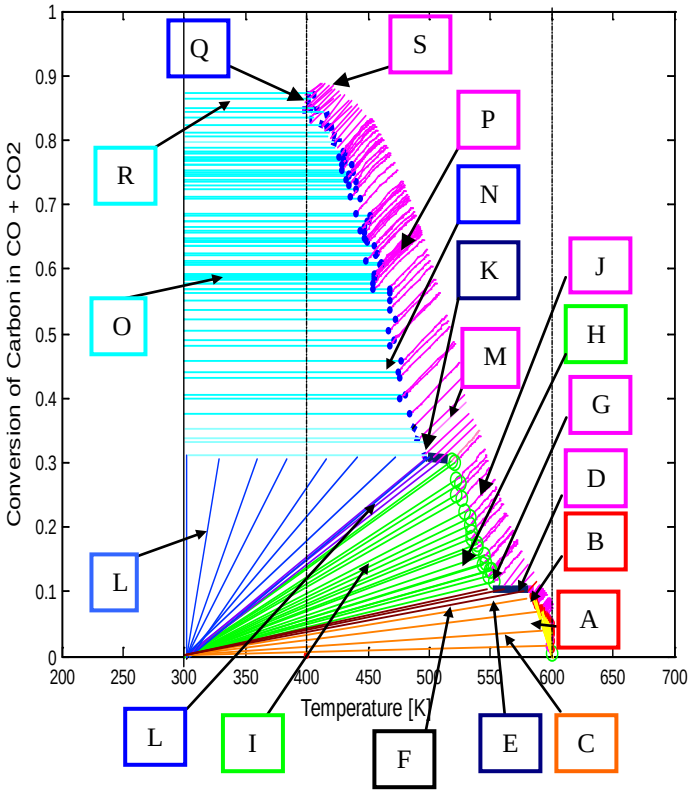


Fig. 9: A Labelled ARC Projection of Methanol Synthesis Case 1

The unit operations sequences for some of the product states in the regions labelled on the $AR^C$ boundary are as follows;

**A** Isothermal DHR

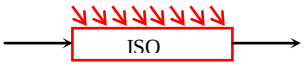


**B** Isothermal DHR with by-pass feed mixing

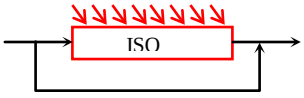


**I** Isothermal DHR - DHR –Cooler – DSR – By-pass feed mixing

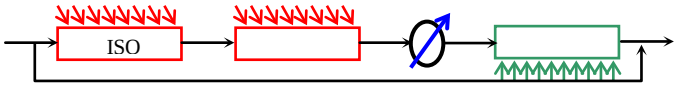


**S** Isothermal DHR - DHR –Cooler – DSR – Cooler – DCR – Isothermal DCR – PFR

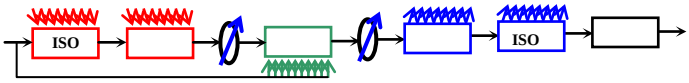


At low conversions (corresponding to the feed), high temperatures are required to influence the dominating water gas shift reaction which is endothermic. This is achieved by an isothermal differentially heated reactor (DHR) operating at a temperature of 600K. An isothermal DHR is essentially a DHR operating with a very large control policy $\theta$, such that the heating process is dominating the reaction process in the combination vector given by equation (19c). There exists a

point where there is a switch from isothermal to a non-isothermal DHR. This switching point is characterised by a sudden decline in the control policy $\theta$, from very large values to moderately low values. This behaviour in the DHR control policy is shown in Figure 10.

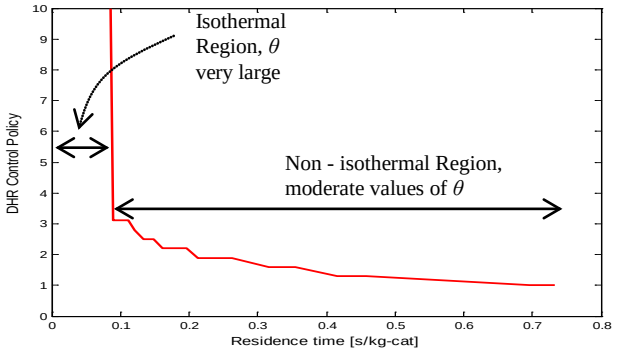


Fig. 10: Variation of the DHR Control Policy with Residence Time

The control policy of this DHR is initially bang-bang in nature as the control policy is kept at the largest value (isothermal region) and suddenly drops to a continuous variation of moderate values (non-isothermal). In continuous region, the control seems to follows a singular arc. The control policy plot is non-smooth with fluctuations, a factor which can be attributed to the inaccuracies of the RCC algorithm computation.

The cooling processes are used to switch from a DHR to a differential side stream reactor (DSR). At this stage the dominating reactions are reactions I and III of methanol formation and the overall reaction system is exothermic. The reaction mixture is optimally cooled by mixing with cold feed to maintain optimum balance between fast rates of reaction and high equilibrium conversion. The DSR control policy $\alpha$, varies with residence time as depicted in Figure 11.

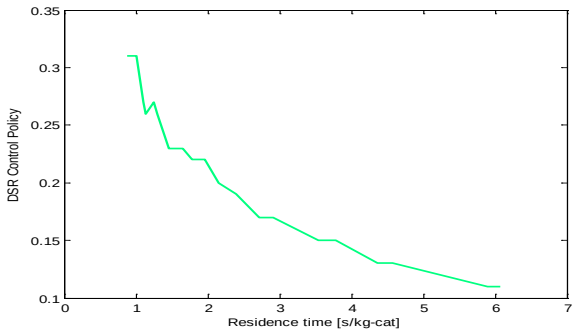


Fig. 11: Variation of the DSR Control Policy with Residence Time

The DSR control policy seems to follow a continuous residence time varying profile. The perturbations in the profile are due to inaccuracies from the RCC algorithm.

The cooling process is applied to switch from a DSR to a differentially cooled reactor (DCR). The DCR follows the optimum cooling profile by combining reaction and cooling such that at any given conversion, reaction occurs at the highest possible rate. The DCR control policy $\beta$, is shown in Figure 12. The non-isothermal DCR control policy follows a smooth continuous arc throughout its entire operation until the minimum catalyst activity temperature is reached. At this point, the control policy takes a sharp discontinuous bend into another continuous arc. This second arc is the isothermal DCR control policy for reaction occurring at a fixed temperature of $T_{min}$ = 400K

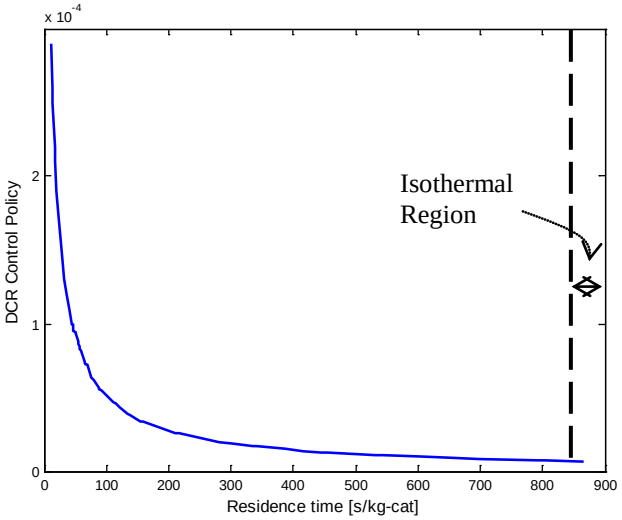


Fig. 12: Variation of the DCR Control Policy with Residence Time

The variation of carbon conversion with residence time as the optimal process combinations are applied is depicted in Figure 13. The structure shown in Figure 13 forms the spine of the $AR^C$ boundary as it gives process combinations for the set of highest carbon conversions at the lowest residence times. All other process operations and/combinations will fall below the convex curve in Figure 13. However, this behaviour is characteristic of the shown projection and is not necessarily true for other projections. The convex process combination curve is formed by the arcs of combinations of reaction and heating (DHR), reaction and mixing (DSR) and reaction and cooling (DSR).

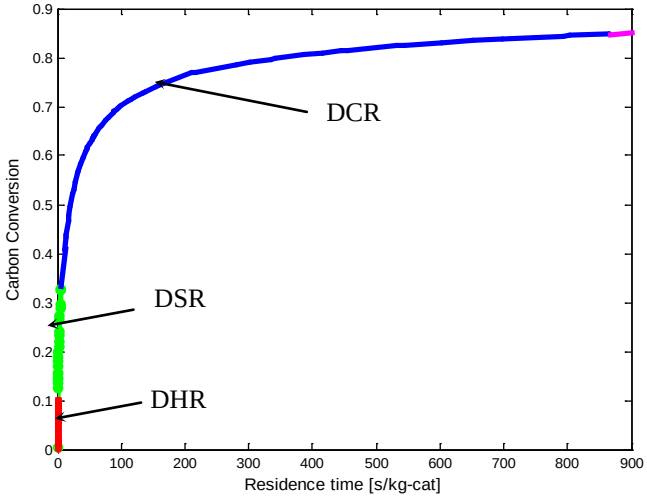


Fig. 13: Carbon Conversion along the Optimal Process Combinations

*B. Case 2*

In the second case we formulate the problem with a varied value of factors, $K_c$ and $K_h$. The factors are still kept equal in magnitude and their value is varied to 10000. This value

indicates that the cooling and heating costs are much cheaper than that of case 1. The two dimensional temperature–carbon conversion projection of the $AR^C$ for this case is depicted in Figure 14. The $AR^C$ shows that a DCR operates in the regions that were previously DSR regions. As the cooling cost decreases, a DCR is preferred to a DSR as it provides lower residence time pathways. There are no visible changes in the DHR profile.

Another visible difference between the two cases is that the switch from a DSR to a DCR in the second case is no longer a cooling process but reaction.

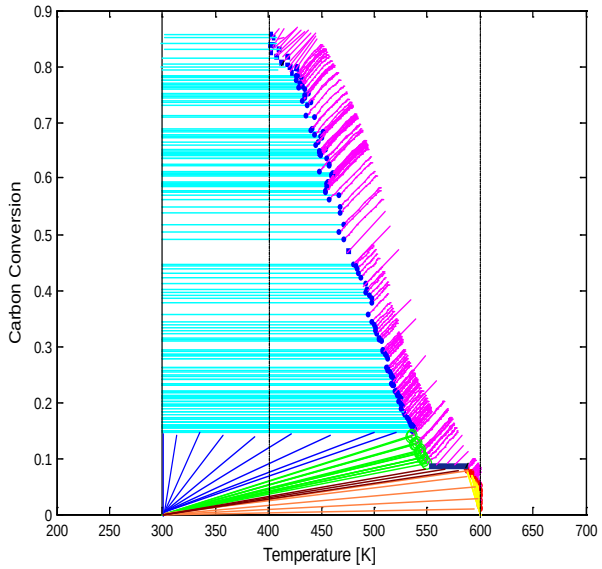


Fig. 14: A 2D T-X $AR^C$ Projection of Methanol Synthesis Case 2

## VI. Discussions

We have used the RCC algorithm to solve the $AR^C$ for methanol synthesis. The product states that shape the $AR^C$ boundary were then interpreted in terms of processes and combinations of processes that are applied to the feed to attain such product states. The control policies for combinations of processes were also obtained by the computation. The methanol synthesis problem has very complex kinetic models and it will not be viable to attain the control policies and solve the $AR^C$ via analytical methods used to study simple problems by Feinberg [7],[8].

For a feed of 1:1 $CO:CO_2$ mole ratio, conversion is generally limited by the low rates of conversion of $CO_2$ to methanol. We demonstrated with the aid of constant rate curves that the reaction rates of $CO_2$ to methanol are in the order of one-tenth of the rates of CO to methanol. The optimal reactor structure obtained via AR analysis takes advantage of the high water-gas-shift activity of the Cu-Zn-Al catalyst. $CO_2$ is shifted to a more active CO by a high temperature DHR. The CO is then converted to methanol by a sequence of DSR and DCRs.

By changing the relative costs of cooling and heating, we showed that the optimal reactor sequence shifts to the favoured application of the lower rate DCR as opposed to DSR. Thus, we have conversely inferred that, as the cooling costs increases, the DSR becomes a more economical (lower residence time) pathway of reaction and cooling as compared to the DCR. As the heating costs are varied, the application of a DHR remains unaffected as it is the only optimal process pathway for combination of reaction and heating to perform the high temperature water-gas-shift of $CO_2$ to CO.

The obtained reactor sequence achieves a 92% conversion of carbon to methanol without the use of excess hydrogen. An advantage that will eliminate the costs associated with excess hydrogen in methanol synthesis processes such as separation and recycling. This also reduces the volume of the reactor as there will be no volume occupied by the excess hydrogen.

## References

[1] Horn, F., (1964), Attainable and non-attainable regions in chemical reaction technique, Proc. Third European Symposium on Chemical Reaction Engineering, Pergamon, New York, pp. 1-10.

[2] Hildebrandt, D. & Glasser, D., (1990), The Attainable Region and Optimal Reactor Structures, Chem. Eng. Sci., 45, (8), pp2161-2168.

[3] Feinberg, M. & Hildebrandt, D., (1997), Optimal Reactor Design from a Geometric Viewpoint: I Universal Properties of the Attainable Region, Chem. Eng. Sci., 52, (10), pp. 1637-1665.

[4] Godorr, S. A. (1998). Optimising chemical reactor structures and other systems by means of the attainable region, PhD thesis, Republic of South Africa: University of the Witwatersrand.

[5] McGregor, C. (1998). Choosing the optimal system structure using the attainable region approach for systems involving reaction and separation, PhD thesis, Republic of South Africa: University of the Witwatersrand.

[6] Nicol, W. (1998). Extending the attainable region technique by including heat exchange and addressing four dimensional problems, PhD thesis, Republic of South Africa: University of the Witwatersrand.

[7] Feinberg, M., (2000 a), Optimal reactor design from a geometric viewpoint II: Critical side-stream reactors., Chem. Eng. Sci., 55, pp. 2455 – 3565.

[8] Feinberg, M., (2000b), Optimal reactor design from a geometric viewpoint III: Critical CFSTRs, Chem. Eng. Sci., 55, pp. 3553 – 2479.

[9] Manousiouthakis, V. I., Justanieah, A. M., & Taylor, L. A. (2004). The Shrink-Wrap algorithm for the construction of the attainable region: An application of the IDEAS framework. Computers & Chemical Engineering, 28, 1563–1575. http://dx.doi.org/10.1016/j.compchemeng.2003.12.005

[10] Abraham, T. K., & Feinberg, M. (2004). Kinetic Bounds on Attainability in the Reactor Synthesis Problem. Industrial & Engineering Chemistry Research, 43, 449–457. http://dx.doi.org/10.1021/ie030497w

[11] Barber, C. B., Dobkin, D. P., & Huhdanpaa, H. T. (1996). The Quickhull algorithm for convex hulls. ACM Transactions on Mathematical Software, 22(4), 469–483. http://dx.doi.org/10.1145/235815.235821

[12] Burri, J. F.,Wilson, S. D.,&Manousiouthakis, V. I. (2000a). Infinite DimEnsionAl Statespace approach to reactor network synthesis: Application to attainable region construction. Computers & Chemical Engineering, 26(6), 849–862.

[13] Kauchali, S., Rooney,W. C., Biegler, L. T., Glasser, D., & Hildebrandt, D. (2002). Linear programming formulations for attainable region analysis. Chemical Engineering Science, 57(11), 2015–2228. http://dx.doi.org/10.1016/S0009-2509(02)00101-X

[14] Kauchali, S., Hausberger, B., Seodigeng, T., Hildebrandt, D., & Glasser, D. (2004). A comparison of automated techniques in determining candidate attainable regions. A case study: The water-gas-shift reaction, ESCAPE-14 Comput. Aided Process Eng., proceedings on the CD-ROM.

[15] Rooney, W. C., Hausberger, B. P., Biegler, L. T., & Glasser, D. (2000). Convex attainable region projections for reactor network synthesis. Computers & Chemical Engineering, 24(2–7), 225–229. http://dx.doi.org/10.1016/S0098-1354(00)00518-4

[16] Zhou, W., & Manousiouthakis, V. I. (2006). Non-ideal reactor network synthesis through IDEAS: Attainable region construction., Chemical Engineering Science, 61, 6936–6945. http://dx.doi.org/10.1016/j.ces.2006.07.002
[17] Seodigeng, T., Hausberger, B., Hildebrandt, D., Glasser, D., (2009). Recursive constant control policy algorithm for attainable regions analysis. Chemical Engineering Science, 33, 309–320.
[18] Natta, G., (1955), Synthesis of methanol, in Catalysis: Hydrogenation and Dehydrogenation (Edited by P. H. Emmett), pp. 349-411, Rheinhold, New York.
[19] Bakemeier, H., Laurer, P. R., Schroder, W., (1970), Development and application of a mathematical model of the methanol synthesis, Chem. Eng Prog. Symp. Ser., 66(98), pp1-10
[20] Leonov, V. E., Karavaev, M. M., Tsybina, E. N., Petrishcheva, G. S., (1973), Kinetics of metanol synthesis on a low- temperature catalyst, Kinet. Katal. 14, pp. 970-975.
[21] Monnier, J. R., Apai, G., Hanrakan, H. J., (1984), Effect of CO2 on the conversion of H2/CO to methanol over copper-chromia catalysts, J. Catal. 88, pp. 523-525.
[22] Chinchen, G. C., Denny, P. J., Parker, D. G., Short, G. D., Spencer, M. S., Waugh, K. C., Whan, D. A., (1984), The activity of copper-zincoxide-aluminiumoxide methanol synthesis catalyst, Prep. Pap. Am. Chem. Soc. Div. Fuel Chem., 29(5), pp178-188
[23] Dybkjaer, I., (1985), Design of ammonia and methanol synthesis reactors, Paper presented at the NATO conference on chemical reactor design and technology, Canada
[24] Denise, B., Sneeden, R. P. A., (1982), Hydrocondensation of carbon dioxide IV., J. Molec. Catal., 17, pp359-366
[25] Graff, G. H., Stamhuis, E. J., Beenackers, A. A. C. M., (1988), Kinetics of low-pressure methanol synthesis, Chem. Eng. Sci. 43, No. 12, pp. 3185-3195
[26] Klier, K., Chatikavanij, V., Herman, R. G., Simmons, G. W., (1982), Catalytic synthesis of methanol from CO/H2. J. Catal., 74, pp. 343-360
[27] Liu, G., Willcox, D., Garland, M., Kung, H. H., (1985), The role of CO2 in methanol synthesis on Cu-Znoxide: an isotope labeling study, J. Catal. 96, pp. 251-260.
[28] Monnier, J. R., Apai, G., Hanrakan, H. J., (1984), Effect of CO2 on the conversion of H2/CO to methanol over copper-chromia catalysts, J. Catal. 88, pp. 523-525.
[29] Struis, R. P. W. J., Stucki, S., Wiedom, M., (1996), A membrane reactor for methanol synthesis, J. Membr. Sci. 113, pp. 93-100
[30] Struis, R. P. W. J., Stucki, S., (2001), Verification of the membrane reactor concept for the methanol synthesis, Applied Catalysis A: General, 216, pp. 117-129
[31] Twigg, V., (1996), Catalyst Handbook, 2nd Ed., Manson Ltd., pp. 293-338,

## LIST OF SYMBOLS AND ABBREVIATIONS

**Abbreviations**

| | |
|---|---|
| AR | Attainable Regions |
| $AR^C$ | Candidate Attainable Regions |
| CFSTR | Continuous Flow Stirred Tank Reactors |
| DCR | Differentially Cooled Reactor |
| DHR | Differentially Heated Reactor |
| DSR | Differential Side-stream Reactor |
| PFR | Plug Flow Reactor |
| RCC | Recursive Constant Control Policy |

**Symbols**

| | |
|---|---|
| $\alpha$ | Combination control policy for fundamental processes (mixing) |
| $\beta$ | Combination control policy for cooling |
| $\theta$ | Combination control policy for cooling |
| $c$ | State variable of the system |
| $c_o$ | State variable of the system at the feeding point |
| $c^*$ | Mixing state variable of the system |
| $f_i$ | Fugacity of gas species $i$ |
| $g(c)$ | General process vector defined at $c$ |
| $h(c)$ | Heating process vector defined at $c$ |
| $k(c)$ | Cooling process vector defined at $c$ |
| $K_c$ | A measure of cooling costs relative to reaction costs |
| $K_i$ | Adsorption equilibrium constant of species $i$ |
| $K^0_{p,j}$ | Chemical equilibrium constant of reaction $j$ based on partial pressure |
| $k_{ps,j}$ | Rate constant of reaction $j$ |
| $m$ | Mass fraction of reaction components |
| $P$ | Partial pressure of the reacting components |
| $\boldsymbol{r}(c)$ | Reaction rate vector defined at $c$ |
| $r'_{i,j}$ | Rate of reaction of species $i$ from reaction $j$ [mol.s$^{-1}$.kg-cat$^{-1}$] |
| R | Universal Gas constant |
| T | Temperature of reaction [K] |
| $T_{ad}$ | Adiabatic temperature gradient |
| $T_c$ | Cooling utility temperature [K] |
| $T_h$ | Heating utility temperature [K] |
| $T_o$ | Feed temperature [K] |
| $\tau$ | Residence time |
| $\upsilon$ | Mixing vector, mixing $c$ with $c^*$ |
| $\Delta H_{rxn}$ | Enthalpy of the reaction |